Electronic Supplementary Information (ESI)

Coordination Distortion Induced Water Adsorption in Hydrophobic Flexible Metal–Organic Frameworks

Yoshinobu Kamakura,[a] Arata Hikawa,[a] Hirofumi Yoshikawa,[b] Wataru Kosaka,[c, d] Hitoshi Miyasaka,[c, d] and Daisuke Tanaka*[a, e]

[a.] *Department of Chemistry, School of Science and Technology, Kwansei Gakuin University, 2-1 Gakuen, Sanda, Hyogo 669-1337, Japan. E-mail: dtanaka@kwansei.ac.jp*

[b.] *Department of Nanotechnology for Sustainable Energy, School of Science and Technology, Kwansei Gakuin University, Sanda, Hyogo 669-1337, Japan*

[c.] *Institute for Materials Research, Tohoku University, 2-1-1 Katahira, Aoba-ku, Sendai 980-8577, Japan*

[d.] *Department of Chemistry, Graduate School of Science, Tohoku University, 6-3 Aramaki-Aza-Aoba, Aoba-ku, Sendai 980-8578, Japan*

[e.] *JST PRESTO, 2-1 Gakuen, Sanda, Hyogo 669-1337, Japan*

Table of Contents

S1. Chemicals and methods used

Chemicals. Cobalt nitrate hexahydrate, nickel nitrate hexahydrate, copper nitrate trihydrate, zinc nitrate hexahydrate, isophthalic acid, and sodium hydroxide were obtained from FUJIFILM Wako Pure Chemical Corporation. Furthermore, 4,4′-bipyridine was purchased from Tokyo Chemical Industry Co., Ltd., and distilled water was obtained from Kishida Chemical Co., Ltd. All the chemicals and solvents used in the study were of reagent grade and used without further purification.

Methods. The X-ray powder diffraction (XRPD) spectra were recorded on a Rigaku MiniFlex600 diffractometer at 40 kV and 15 mA using a Cu-target tube. The samples were examined without grinding, and the data were collected for 2θ values of 3°–30° using Cu–Kα radiation. The diffraction patterns were obtained in an Ar atmosphere using an air-sensitive sample holder purchased from Rigaku. Thermogravimetry (TG) was performed on a SHIMADZU DTG-60 instrument over a temperature range of 30–150 °C at 5 °C min^{-1} in air. Scanning electron microscopy (SEM) images and SEM-energy-dispersive X-ray spectroscopy (SEM-EDX) maps were captured on a JEOL JCM-6000 system equipped with an EDX analyzer (EX-37001) and DX200s detector. Magnetic susceptibility experiments were performed using a SQUID magnetometer (MPMS–7XL, Quantum Design Ltd.) in the temperature range 1.8–300 K under a direct current field of 1000 T. The XRPD patterns were simulated based on single-crystal data using the diffraction crystal module of the software program Mercury (version 3.9), which are available free of charge via the Internet at http://www.iucr.org.

Determination of crystal structure. The crystallographic data for CuCID-1 were collected with a CCD diffractometer using Mo–Kα radiation. The CrystalClear-SM Expert 2.0 r2 program (Rigaku, 2009) was used for integrating the diffraction profiles. The crystal structures were solved by directed methods using the program SHELXT and refined using SHELXL. Anisotropic thermal parameters were used to refine all the non-H atoms (CCDC number: 1978140)

H_2O-sorption isotherms. H_2O-sorption isotherms were acquired on a MicrotracBEL BELSORP-max volumetric gas adsorption measurement system. The samples were dried under reduced pressure at 120 °C for 72 h prior to any experiment.

S2. Synthesis methods

Synthesis of disodium isophthalic acid (Na_2ip). Sodium hydroxide (2.5 g, 0.6 mol) was dissolved in a minimal amount of water. Isophthalic acid (5.0 g, 0.3 mol) was added to the mixture, which was then sonicated and heated at 50 °C to ensure complete dissolution. After the dissolution process, excess ethanol was added. The residue was filtered and dried under reduced pressure at 120 °C overnight, yielding a white powder.

Synthesis of CoCID-1. $Co(NO_3)_2{\cdot}6H_2O$ (116.4 mg, 0.40 mmol) was dissolved in water (8.0 mL). Next, Na_2ip (84.0 mg, 0.40 mmol) and bpy (62.5 mg, 0.40 mmol) were added to the solution, which was sealed in a 15-mL Teflon-lined stainless-steel container and heated at 150 °C for 48 h. The M:ip:bpy molar ratio was 1:1:1. After the heating process, the container was cooled to 30 °C at a rate of 10 °C h^{-1}. The residue was washed with MeOH and filtered, yielding an orange-red crystalline powder with a yield of 79%.

Synthesis of NiCID-1. The synthesis procedure was similar to that for CoCID-1 with the exception that $Co(NO_3)_2{\cdot}6H_2O$ (116.4 mg, 0.40 mmol) was replaced by $Ni(NO_3)_2{\cdot}6H_2O$ (116.3 mg, 0.40 mmol). A light-green crystalline powder was obtained with a yield of 92%.

Synthesis of CuCID-1⊃H_2O. The synthesis procedure was similar to that for CoCID-1 with the exception that $Co(NO_3)_2{\cdot}6H_2O$ (116.4 mg, 0.40 mmol) was replaced by $Cu(NO_3)_2{\cdot}3H_2O$ (96.6 mg, 0.40 mmol). A light-blue crystalline powder was obtained with a yield of 95%.

Synthesis of ZnCID-1⊃H_2O. The synthesis procedure was similar to that for CoCID-1 with the exception that $Co(NO_3)_2{\cdot}6H_2O$ (116.4 mg, 0.40 mmol) was replaced by $Zn(NO_3)_2{\cdot}6H_2O$ (119.0 mg, 0.40 mmol). A colorless crystalline powder was obtained with a yield of 73%.

Synthesis of $Co_{0.5}Ni_{0.5}$CID-1. The following two aqueous solutions were prepared: $Co(NO_3)_2{\cdot}6H_2O$ (72.8 mg, 0.40 mmol) dissolved in water (5.0 ml) and $Ni(NO_3)_2{\cdot}6H_2O$ (72.7 mg, 0.40 mmol) dissolved in

water (5.0 ml). Next, the two solutions were mixed with Na_2ip (84.0 mg, 0.40 mmol) and bpy (62.5 mg, 0.40 mmol), and the mixture was placed in a 15-mL Teflon-lined stainless-steel container and heated at 150 °C for 48 h. Subsequently, the container was cooled to room temperature at a rate of 10 °C h^{-1}. The residue was washed with MeOH and filtered, yielding a light-blown crystalline powder (Coaq:Niaq = x:1−x).

Synthesis of Co_xCu_{1-x}CID-1 (x = 0.15, 0.33, 0.50, 0.67, and 0.85). The following two aqueous solutions were prepared: $Co(NO_3)_2{\cdot}6H_2O$ (320.1 mg, 0.40 mmol) dissolved in water (22.0 mL) and $Cu(NO_3)_2{\cdot}3H_2O$ (265.8 mg, 0.40 mmol) dissolved in water (22.0 mL). Next, the two solutions were mixed with Na_2ip (84.0 mg, 0.40 mmol) and bpy (62.5 mg, 0.40 mmol), and the mixture was placed in a 15-mL Teflon-lined stainless-steel container and heated at 150 °C for 48 h. The Zn:Co:ip:bpy molar ratio was x:1−x:1:1, and the Znaq:Coaq volume ratio was x:1−x. The total volume was 8.0 mL. Subsequently, the container was cooled to room temperature at a rate of 10 °C h^{-1}. Then, the residue was washed with MeOH and filtered, yielding a light-blown crystalline powder (Coaq:Niaq = x:1−x).

Synthesis of Co_xZn_{1-x}CID-1 (x = 0.15, 0.33, 0.50, and 0.67). The synthesis procedure was similar to that for Co_xCu_{1-x}CID-1 with the exception that $Cu(NO_3)_2{\cdot}3H_2O$ (265.8 mg, 0.40 mmol) was replaced by $Zn(NO_3)_2{\cdot}6H_2O$ (327.3 mg, 0.40 mmol). A light-peach crystalline powder was obtained.

Synthesis of Ni_xCu_{1-x}CID-1 (x = 0.15, 0.33, 0.50, 0.67, and 0.85). The synthesis procedure was similar to that for Co_xCu_{1-x}CID-1 with the exception that $Co(NO_3)_2{\cdot}6H_2O$ (320.1 mg, 0.40 mmol) was replaced by $Ni(NO_3)_2{\cdot}6H_2O$ (319.9 mg, 0.40 mmol). A light-blue crystalline powder was obtained.

Synthesis of Ni_xZn_{1-x}CID-1 (x = 0.15, 0.33, 0.50, and 0.67). The synthesis procedure was similar to that for Co_xCu_{1-x}CID-1 with the exception that $Co(NO_3)_2{\cdot}6H_2O$ (320.1 mg, 0.40 mmol) and $Cu(NO_3)_2{\cdot}3H_2O$ (265.8 mg, 0.40 mmol) were replaced by $Ni(NO_3)_2{\cdot}6H_2O$ (319.9 mg, 0.40 mmol) and $Zn(NO_3)_2{\cdot}6H_2O$ (327.4 mg, 0.40 mmol), respectively. A light-green crystalline powder was obtained.

Synthesis of Cu_xZn_{1-x}CID-1 (x = 0.15, 0.33, 0.50, 0.67, and 0.85). The synthesis procedure was similar to that for Co_xCu_{1-x}CID-1 with the exception that $Co(NO_3)_2{\cdot}6H_2O$ (320.1 mg, 0.40 mmol) and $Cu(NO_3)_2{\cdot}3H_2O$ (265.8 mg, 0.40 mmol) were replaced by $Cu(NO_3)_2{\cdot}3H_2O$ (265.8 mg, 0.40 mmol) and $Zn(NO_3)_2{\cdot}6H_2O$ (327.2 mg, 0.40 mmol), respectively. A light-blue crystalline powder was obtained.

Synthesis of $Co_{0.5}Ni_{0.5}$CID-1_H using half the amount of the ligand. The synthesis procedure was similar to that for $Co_{0.5}Ni_{0.5}$CID-1 with the exception that the Co:Ni:ip:bpy molar ratio was changed to 1:1:1:1. A light-blown crystalline powder was obtained.

Synthesis of $Co_{0.5}Cu_{0.5}$CID-1_H using half the amount of the ligand. The synthesis procedure was similar to that for $Co_{0.5}Ni_{0.5}$CID-1_H with the exception that $Ni(NO_3)_2{\cdot}6H_2O$ (72.7 mg, 0.40 mmol) was replaced by $Cu(NO_3)_2{\cdot}4H_2O$ (60.4 mg, 0.40 mmol). A light-blue crystalline powder was obtained.

Synthesis of $Co_{0.5}Zn_{0.5}$CID-1_H using half the amount of the ligand. The synthesis procedure was similar to that for $Co_{0.5}Ni_{0.5}$CID-1_H with the exception that $Ni(NO_3)_2{\cdot}6H_2O$ (72.7 mg, 0.40 mmol) was replaced by $Zn(NO_3)_2{\cdot}6H_2O$ (74.4 mg, 0.40 mmol). A light-pink crystalline powder was obtained.

Synthesis of $Ni_{0.5}Cu_{0.5}$CID-1_H using half the amount of the ligand. The synthesis procedure was similar to that $Co_{0.5}Ni_{0.5}$CID-1_H with the exception that $Co(NO_3)_2{\cdot}6H_2O$ (72.8 mg, 0.40 mmol) and $Ni(NO_3)_2{\cdot}6H_2O$ (72.7 mg, 0.40 mmol) were replaced by $Ni(NO_3)_2{\cdot}6H_2O$ (72.7 mg, 0.40 mmol) and $Cu(NO_3)_2{\cdot}3H_2O$ (60.4 mg, 0.40 mmol), respectively. A light-blue crystalline powder was obtained.

Synthesis of $Ni_{0.5}Zn_{0.5}$CID-1_H using half the amount of the ligand. The synthesis procedure was similar to that for $Co_{0.5}Ni_{0.5}$CID-1_H with the exception that $Co(NO_3)_2{\cdot}6H_2O$ (72.8 mg, 0.40 mmol) and $Ni(NO_3)_2{\cdot}6H_2O$ (72.7 mg, 0.40 mmol) were replaced by $Ni(NO_3)_2{\cdot}6H_2O$ (72.7 mg, 0.40 mmol) and $Zn(NO_3)_2{\cdot}6H_2O$ (74.4 mg, 0.40 mmol), respectively. A light-green crystalline powder was obtained.

Synthesis of $Cu_{0.5}Zn_{0.5}$CID-1_H using half the amount of the ligand. The synthesis procedure was similar to that for $Co_{0.5}Ni_{0.5}$CID-1_H with the exception that $Co(NO_3)_2{\cdot}6H_2O$ (72.8 mg, 0.40 mmol) and $Ni(NO_3)_2{\cdot}6H_2O$ (72.7 mg, 0.40 mmol) were replaced by $Cu(NO_3)_2{\cdot}3H_2O$ (60.4 mg, 0.40 mmol) and $Zn(NO_3)_2{\cdot}6H_2O$ (74.4 mg, 0.40 mmol), respectively. A light-blue crystalline powder was obtained.

Degassing treatment of CID-1. The as-synthesized CID-1 was washed with MeOH and dried *in vacuo* overnight at 120 °C.

S3. XRPD patterns of the as-synthesized MCID-1 compounds

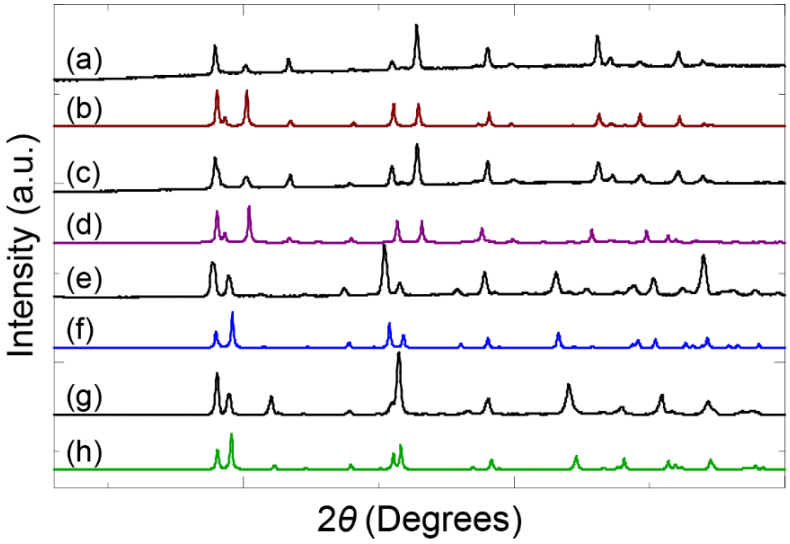

Fig. S1. XRPD patterns of (a) as-synthesized CoCID-1, (b) CoCID-1 (simulated†),[1] (c) as-synthesized NiCID-1, (d) NiCID-1 (simulated†),[2] (e) as-synthesized CuCID-1, (f) CuCID-1⊃H_2O (simulated†),[3] (g) as-synthesized ZnCID-1, and (h) ZnCID-1⊃H_2O (simulated†).[4] (†Note: b, d, f, and h are simulated profiles from single-crystal data).

S4. Crystal structures of the MCID-1 compounds

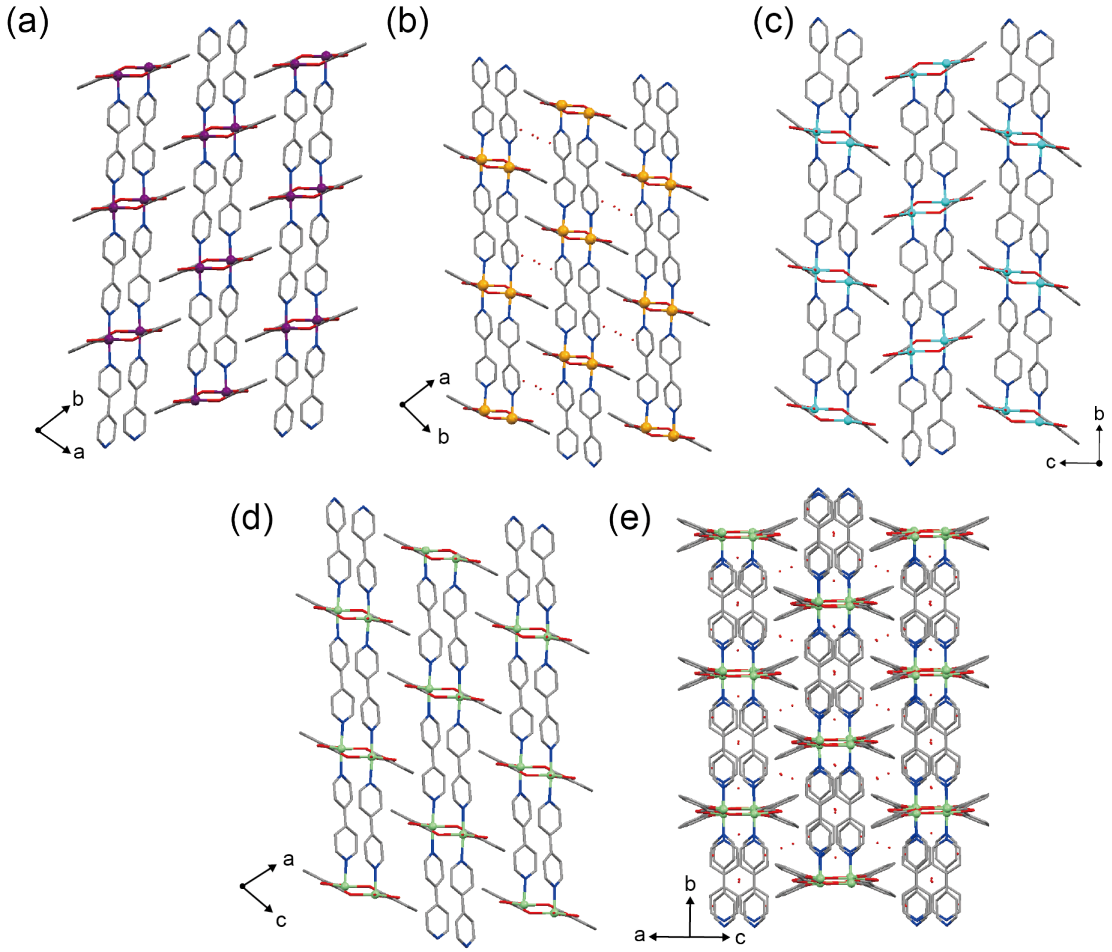

Fig. S2. Crystal structures of (a) NiCID-1, (b) CoCID-1⊃H_2O,[5] (c) CuCID-1, (d) ZnCID-1, and (e) ZnCID-1⊃H_2O. Purple, orange, light blue, light green, gray, blue, and red represent Ni, Co, Cu, Zn, C, N, and O, respectively. H atoms are omitted for clarity.

S5. Thermogravimetric curves

We measured the TG curves to evaluate the number of water molecules in the as-synthesized MCID-1. For ZnCID-1, the sample was exposed to water vapor for 1 h prior to the experiment because ZnCID-1 easily desorbs guest molecules under ambient conditions, e.g., during filtration. The TG curves indicated that CoCID-1 and NiCID-1 did not contain water molecules, whereas CuCID-1 and ZnCID-1 displayed weight loss of 11.7% and 11.8%, respectively, corresponding to water evaporation. These values indicate that CuCID-1 and ZnCID-1 both contained 2.9 water molecules per cell unit, although the cif files indicate that MCID-1 (M = Cu and Zn) each contain three water molecules per cell unit. This inconsistency is considered to be caused by desorption of water molecules from the cavity into the air before the TG measurement.

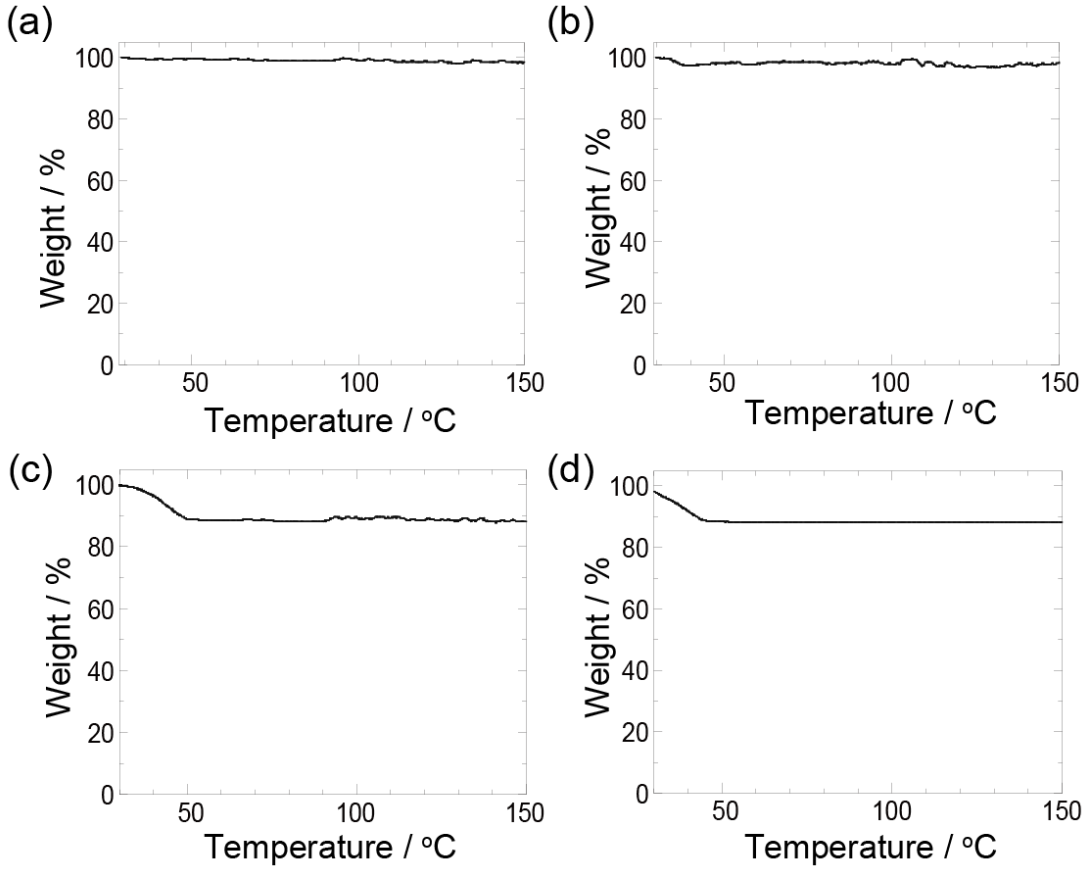

Fig. S3. TG curves of (a) CoCID-1, (b) NiCID-1, (c) CuCID-1, and (d) ZnCID-1.

S6. XRPD patterns of MCID-1 after degassing treatment

The crystal structures of both CoCID-1 and CoCID-1⊃H_2O have been reported previously.[1,5] Their assembled structures, however, are almost the same except for the presence of water molecules in the pores (Figs. 1b and S2b). The values of their crystallographic parameters are almost the same; both are in the *P*-1 space group, and they have 0D hydrophobic pores, suggesting that water inclusion in CoCID-1 is not accompanied by a framework structural transformation. Under our synthesis conditions, the XRPD patterns of the as-synthesized CoCID-1 sample is similar to that of CoCID-1 devoid of water molecules (Fig. S4).

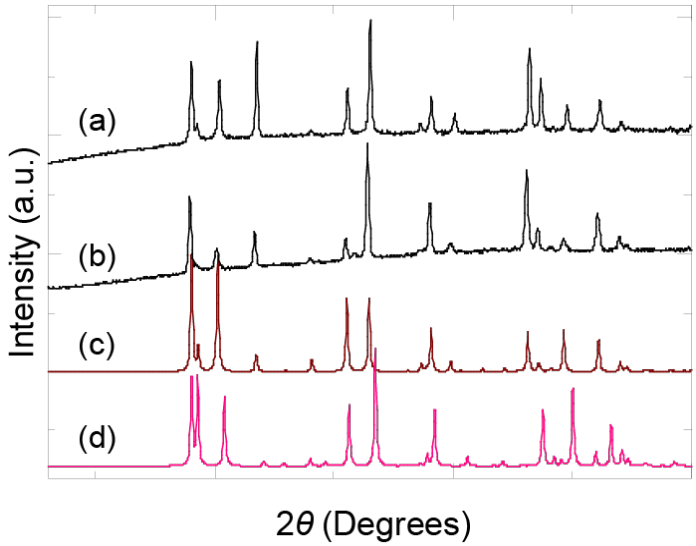

Fig. S4. XRPD patterns of (a) degassed CoCID-1, (b) as-synthesised CoCID-1, (c) CoCID-1 (simulated†), and (d) CoCID-1⊃H_2O (simulated†). (†Note: c and d are simulated profiles from single crystal data).

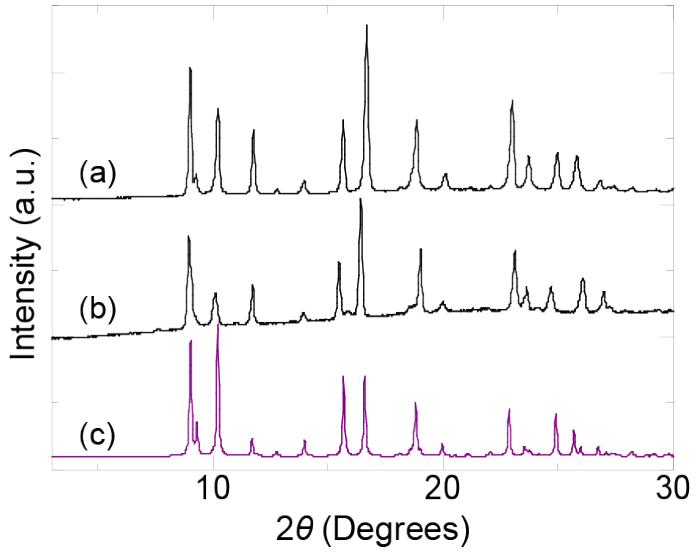

Fig. S5. XRPD patterns of (a) degassed NiCID-1, (b) as-synthesised NiCID-1, and (c) NiCID-1 (simulated profile from single crystal data).

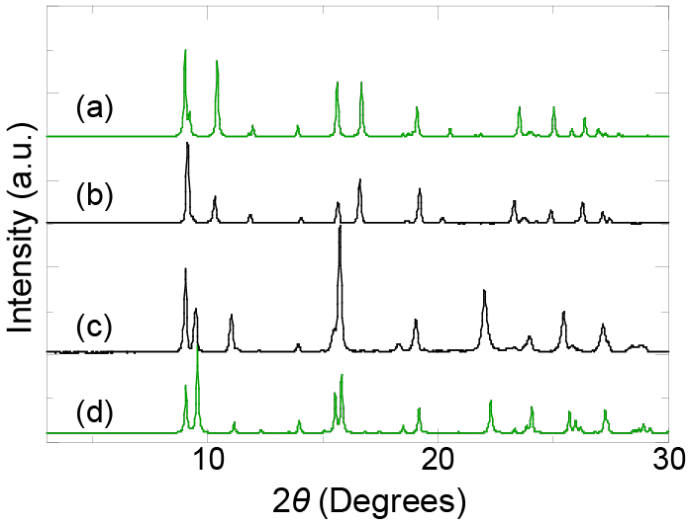

Fig. S6. XRPD patterns of (a) ZnCID-1 (simulated†), (b) degassed ZnCID-1, (c) as-synthesised ZnCID-1, and (d) ZnCID-1⊃H_2O (simulated†). (†Note: a and d are simulated profiles from single crystal data).

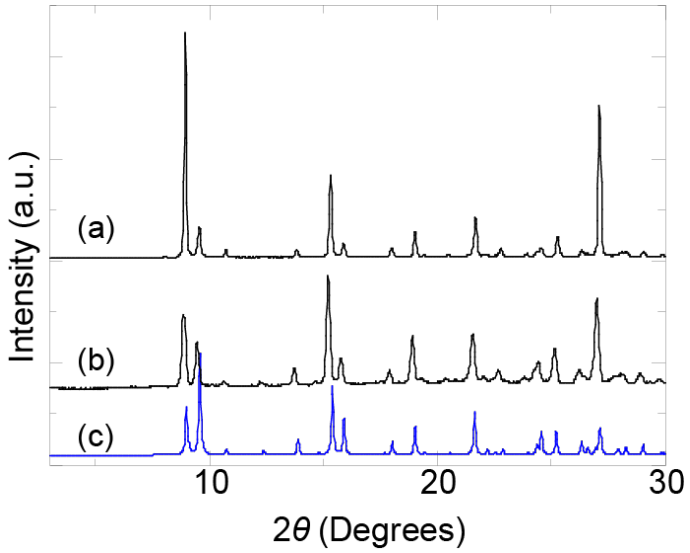

Fig. S7. XRPD patterns of (a) degassed CuCID-1, (b) as-synthesised CuCID-1, and (c) CuCID-1⊃H_2O (simulated profile from single crystal data).

S7. Crystallographic data (CCDC: 1978140)

Table S1. Crystallographic data and parameters for CuCID-1

Compound	CuCID-1
Formula	$C_{18}H_{12}N_2O_4Cu$
Formula weight	383.84
Temperature (K)	200
Crystal system	Monoclinic
Space group	$P2_1/c$
a (Å)	10.111(2)
b (Å)	11.154(2)
c (Å)	15.896(4)
β (°)	104.510(9)
Volume (Å^3)	1735.54
Z	4
ρ_{calc} (g cm^{-3})	1.469
μ (mm^{-1})	1.282
F(000)	780
Wavelength/Å	0.71075
2θ range for data collection/°	2.081 to 27.500
Index ranges	$-13 \leq h \leq 13$
	$-14 \leq k \leq 14$
	$-20 \leq l \leq 20$
Reflection collected	19670
Unique reflections	2233
Goodness-of-Fit on F^2	1.043
Final R_1 index [I ≥ 2σ (I)]	0.0918
Final R_1 index [all data]	0.1937
Final wR_2 index [I ≥ 2σ (I)]	0.1978
Final wR_2 index [all data]	0.2758
Largest diff. peak/hole / (e Å^{-3})	0.853/−1.259

S8. Space groups and bond lengths of the MCID-1 compounds

Table S2. Space groups and bond lengths of MCID-1

Compound	Space Group	Bond Length / Å					
		M-O1	M-O2	M-O3	M-O4	M-N1	M-N2
CoCID-1	*P* -1	2.12	2.25	2.01	2.05	2.16	2.16
NiCID-1	*P* -1	2.12	2.18	2.03	2.06	2.11	2.11
CuCID-1	$P\,2_1/c$	2.01	2.57	1.99	2.23	2.03	2.04
ZnCID-1	*P* -1	2.13	2.32	2.04	2.06	2.15	2.18
CuCID-1 ⊃ H_2O	*C* 2/c	2.04	2.64	1.97	2.23	2.02	2.03
ZnCID-1 ⊃ H_2O	*C* 2/c	2.08	2.57	2.04	2.06	2.15	2.15

S9. Time-resolved XRPD patterns of CuCID-1

The diffraction patterns were recorded in an Ar atmosphere using an air-sensitive sample holder after degassing (0 min). The sample was subsequently exposed to air (293 K, RH = 55%).

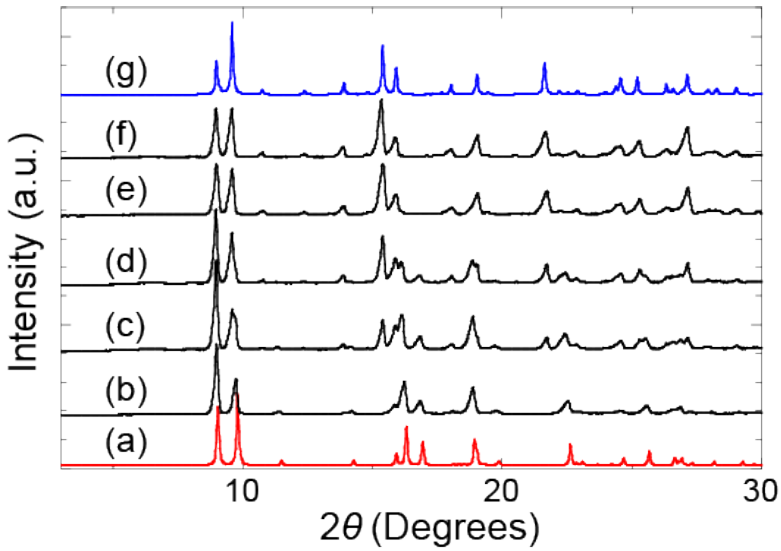

Fig. S8. Time-resolved XRPD patterns of (a) CuCID-1 (simulated†); CuCID-1 after exposure to air for (b) 0 min (degassed), (c) 5 min, (d) 10 min, (e) 20 min, and (f) 30 min; and (g) CuCID-1⊃H_2O (simulated†). (†Note: a and g are simulated profiles from single crystal data).

S10. Pore properties of MCID-1

We calculated the pore properties of MCID-1 to evaluate the effect of the type of metal ion. The calculations indicate that the cavity volumes of MCID-1 (M = Co, Ni, Cu, and Zn) are 12.5% (108.5 Å^3), 11.5% (99.7 Å^3), 12.2% (212.5 Å^3), and 11.2% (95.4 Å^3) per cell volume, respectively. It is noted that *Z* value of CuCID-1 is four, whereas that of MCID-1 is two. The cavity sizes of MCID-1 (M = Co, Ni, Cu, and Zn) are 6 × 7 × 4 Å^3, 6 × 7 × 4 Å^3, 6 × 7 × 4 Å^3, and 6 × 7 × 4 Å^3, respectively. The pore percentages per cell volume are similar, and the pore structure and surroundings are almost the same regardless of the metal ion. The major differences in porosity and structural properties of MCID-1 is the coordination distortion, as shown in Table S2. These results suggest that the cavity of MCID-1 is not significantly affected by the metal ion species, whereas the water-adsorption properties are strongly affected by the coordination distortion.

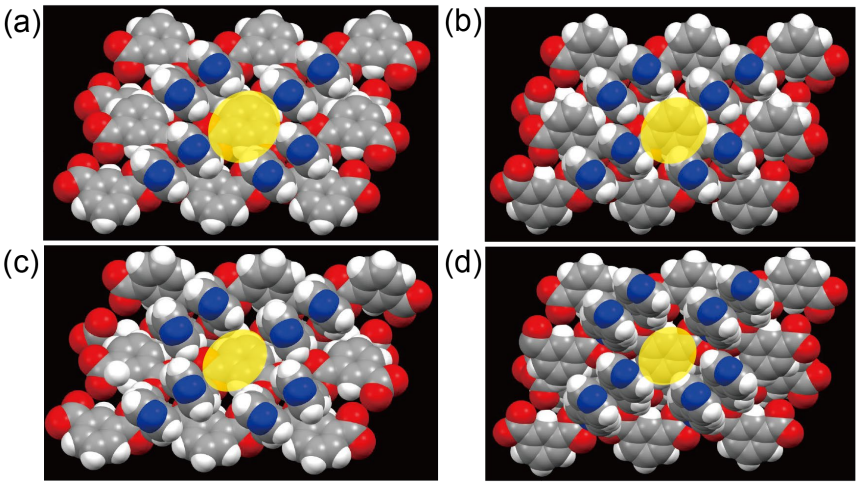

Fig. S9. Pore surroundings of MCID-1. (a) CoCID-1, (b) NiCID-1, (c) CuCID-1, and (d) ZnCID-1. Gray, blue, red, and white represent C, N, O, and H respectively. H atoms are omitted for clarity. Cavities are highlighted by the yellow circles.

S11. Coordination and water network structures of ZnCID-1

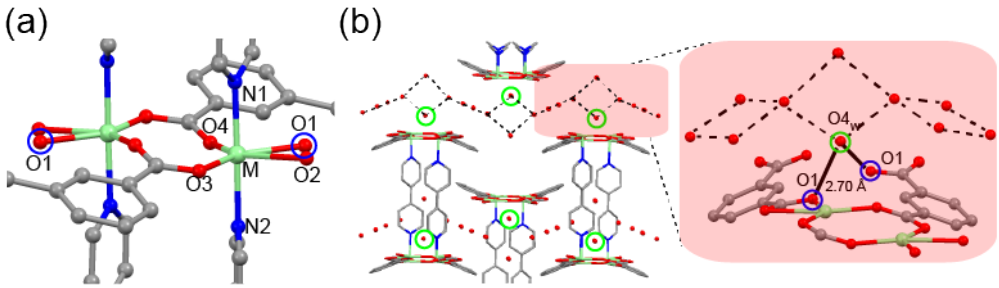

Fig. S10. (a) Coordination structure of ZnCID-1 and (b) structure of the water network in the 1D channel.

S12. XRPD patterns of $M1_{0.5}M2_{0.5}$CID-1

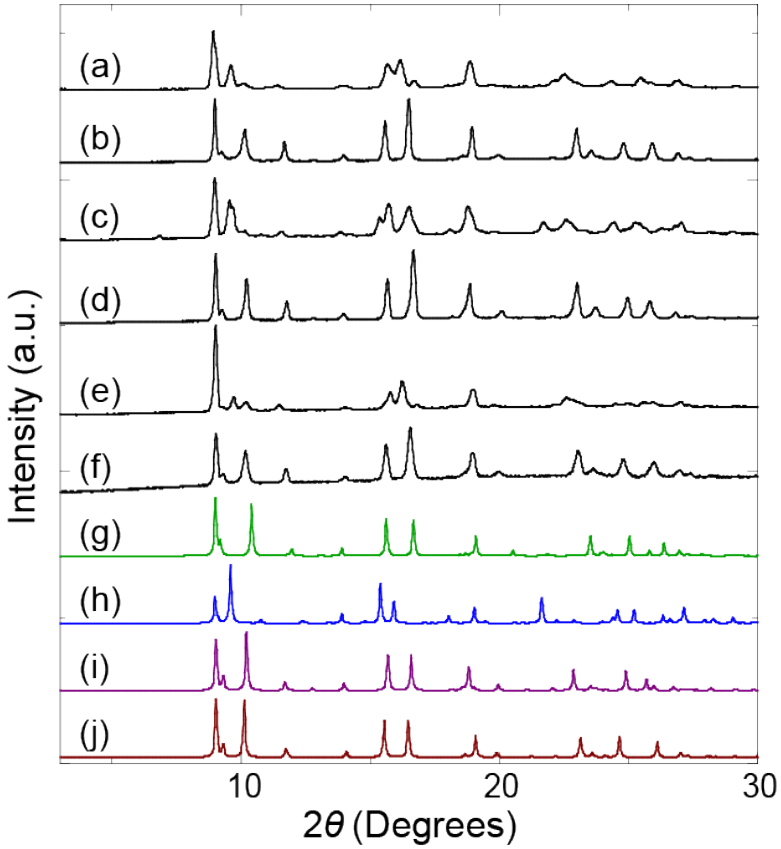

Fig. S11. XRPD patterns of (a) as-synthesised $Zn_{0.5}Cu_{0.5}$CID-1, (b) as-synthesised $Zn_{0.5}Ni_{0.5}$CID-1, (c) as-synthesised $Cu_{0.5}Ni_{0.5}$CID-1, (d) as-synthesised $Zn_{0.5}Co_{0.5}$CID-1, (e) as-synthesised $Co_{0.5}Cu_{0.5}$CID-1, (f) as-synthesised $Ni_{0.5}Co_{0.5}$CID-1; and (g) ZnCID-1 ⊃ H_2O (simulated†), (h) CuCID-1⊃H_2O (simulated†), (i) NiCID-1 (simulated†), (j) CoCID-1 (simulated†). (†Note: g–j are simulated profiles from single crystal data).

S13. Evaluating XRPD patterns of the $M1_{0.5}M2_{0.5}CID\text{-}1_H$ compounds

We synthesized solid-solution-type $M1_{0.5}M2_{0.5}CID\text{-}1_H$ using half the amount of the ligand (M1:M2:Na_2ip:bpy = 1:1:1:1). The XRPD patterns and SEM-EDX maps indicated that the patterns of $M1_{0.5}M2_{0.5}CID\text{-}1_H$ are similar, with the exception of $M_{0.5}Cu_{0.5}CID\text{-}1_H$, which only show peaks related to CuCID-1 (Figs. S12 and S13). Therefore, we surmise that CuCID-1 crystallized more rapidly than the other compounds in water because CuCID-1 ⊃ H_2O is very stable.

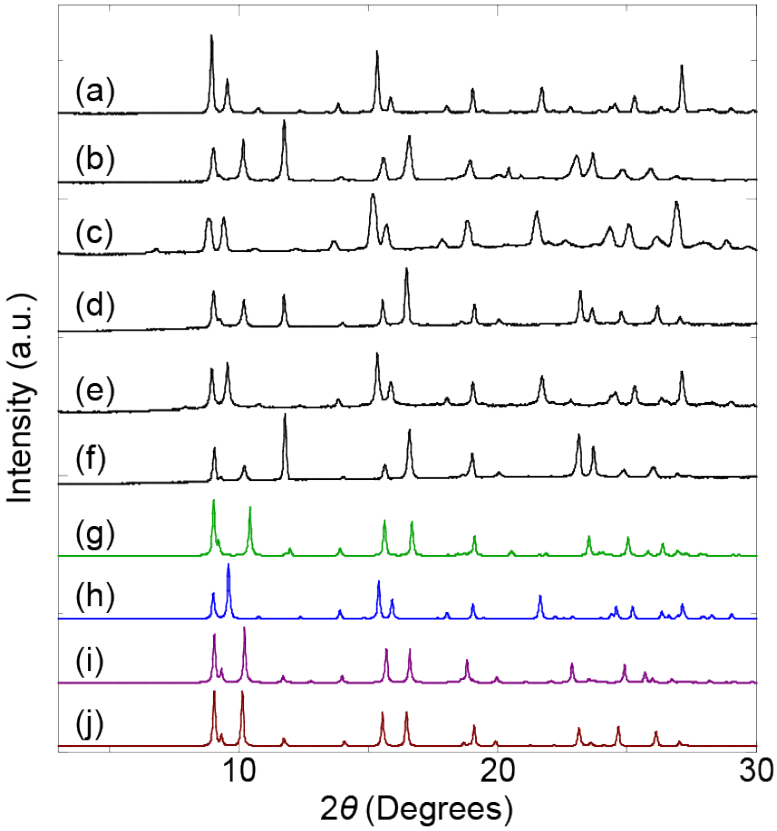

Fig. S12. XRPD patterns of (a) as-synthesised $Zn_{0.5}Cu_{0.5}CID\text{-}1_H$, (b) as-synthesised $Zn_{0.5}Ni_{0.5}CID\text{-}1_H$, (c) as-synthesised $Cu_{0.5}Ni_{0.5}CID\text{-}1_H$, (d) as-synthesised $Zn_{0.5}Co_{0.5}CID\text{-}1_H$, (e) as-synthesised $Co_{0.5}Cu_{0.5}CID\text{-}1_H$; (f) as-synthesised $Ni_{0.5}Co_{0.5}CID\text{-}1_H$ produced using half the amount of ligand; and (g) ZnCID-1 ⊃ H_2O (simulated†), (h) CuCID-1 ⊃ H_2O (simulated†), (i) NiCID-1 (simulated†), (j) CoCID-1 (simulated†). (†Note: g–j are simulated profiles from single crystal data).

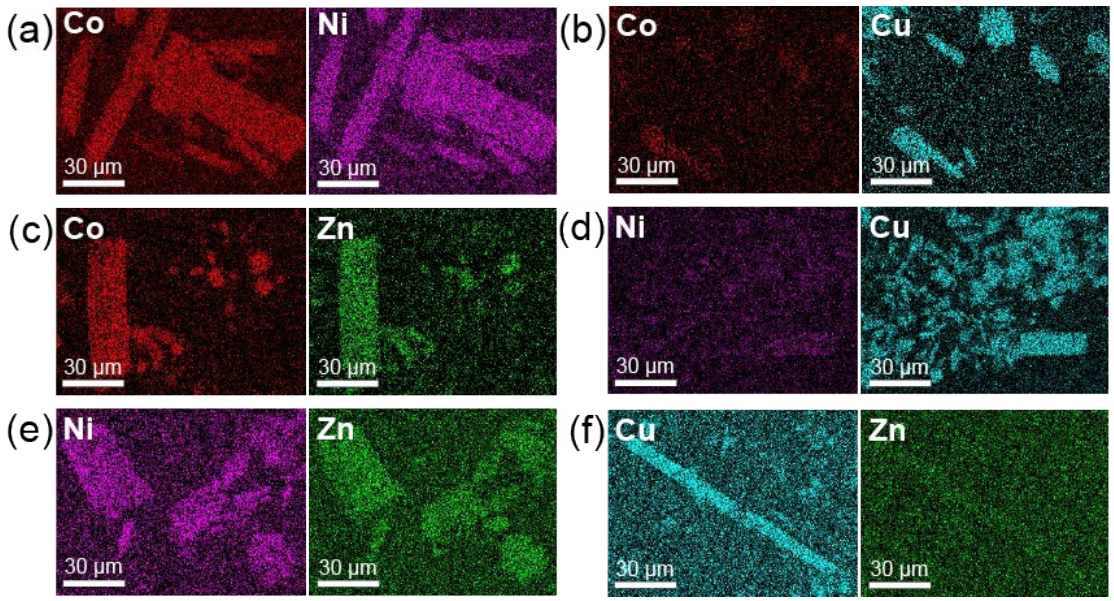

Fig. S13. SEM-EDX maps of (a) $Ni_{0.5}Co_{0.5}$CID-1, (b) $Co_{0.5}Cu_{0.5}$CID-1, (c) $Zn_{0.5}Co_{0.5}$CID-1, (d) $Ni_{0.5}Co_{0.5}$CID-1, (e) $Zn_{0.5}Ni_{0.5}$CID-1, and (f) $Zn_{0.5}Cu_{0.5}$CID-1_H synthesised using half the amount of ligand.

S14. Evaluating the XRPD patterns of the $M1_xM2_{1-x}$CID-1 compounds

The XRPD patterns and SEM-EDX maps of $M1_xM2_{1-x}$CID-1 (x = 0.15, 0.33, 0.67, and 0.85) are similar to those obtained when x = 0.50. However, the products did not mix well when Cu ions are used to prepare solid-solution-type CID-1 (Figs. S14–S23).

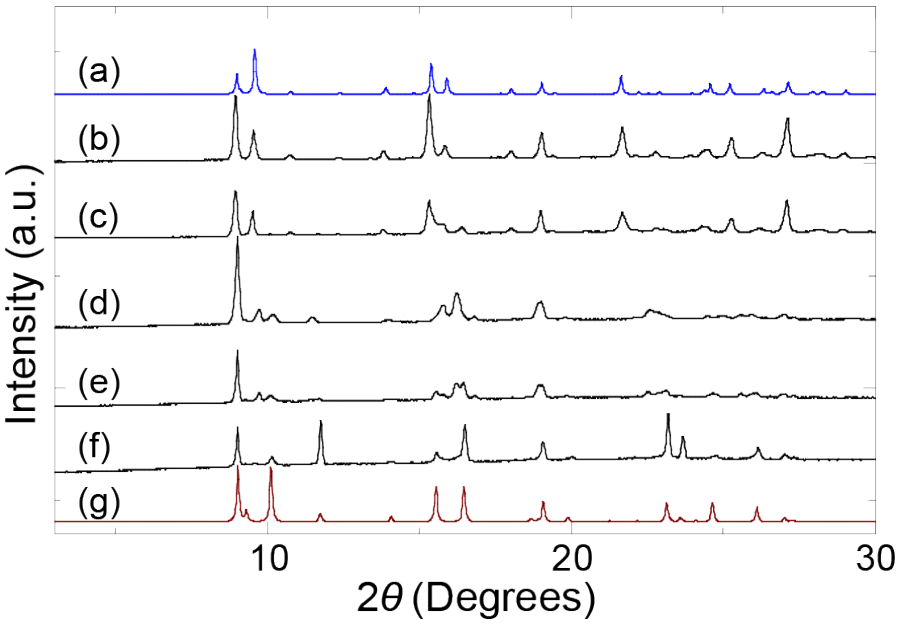

Fig. S14. XRPD patterns of (a) CuCID-1⊃H_2O (simulated†); Co_xCu_{1-x}CID-1 with (b) x = 0.15, (c) x = 0.33, (d) x = 0.50, (e) x = 0.67, and (f) x = 0.85; and (g) CoCID-1 (simulated†). (†Note: a and g are simulated profiles from single crystal data).

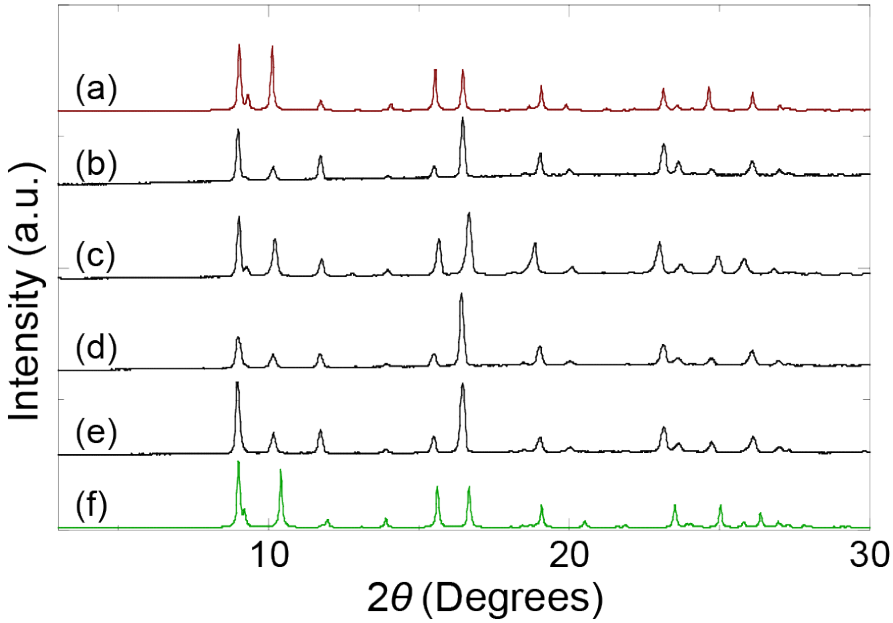

Fig. S15. XRPD patterns of (a) CoCID-1 (simulated†); Zn_xCo_{1-x}CID-1 with (b) x = 0.33, (c) x = 0.50, (d) x = 0.67, and (e) x = 0.85; and (f) ZnCID-1 (simulated†). (†Note: a and f are simulated profiles from single crystal data).

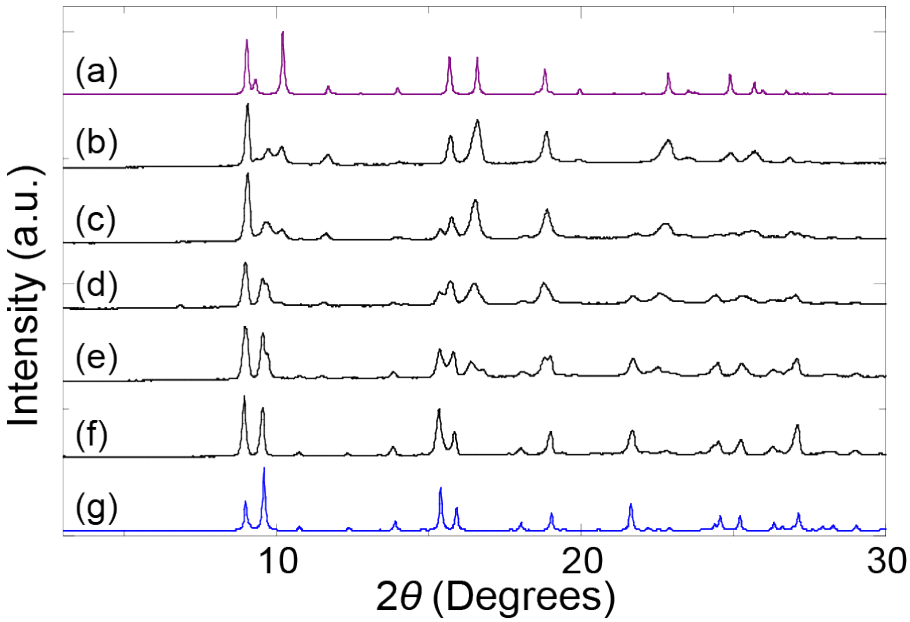

Fig. S16. XRPD patterns of (a) NiCID-1 (simulated†); Cu_xNi_{1-x}CID-1 with (b) x = 0.15, (c) x = 0.33, (d) x = 0.50, (e) x = 0.67, and (f) x = 0.85; and (g) CuCID-1⊃H_2O (simulated†). (†Note: a and g are simulated profiles from single crystal data).

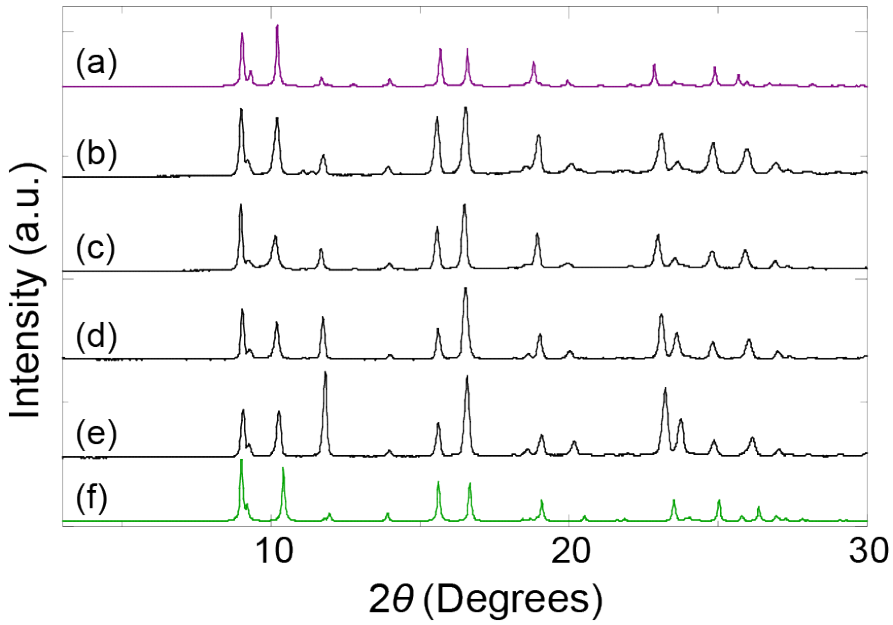

Fig. S17. XRPD patterns of (a) NiCID-1 (simulated†); Zn_xNi_{1-x}CID-1 with (b) x = 0.33, (c) x = 0.50, (d) x = 0.67, and (e) x = 0.85; and (f) ZnCID-1 (simulated†). (†Note: a and f are simulated profiles from single crystal data).

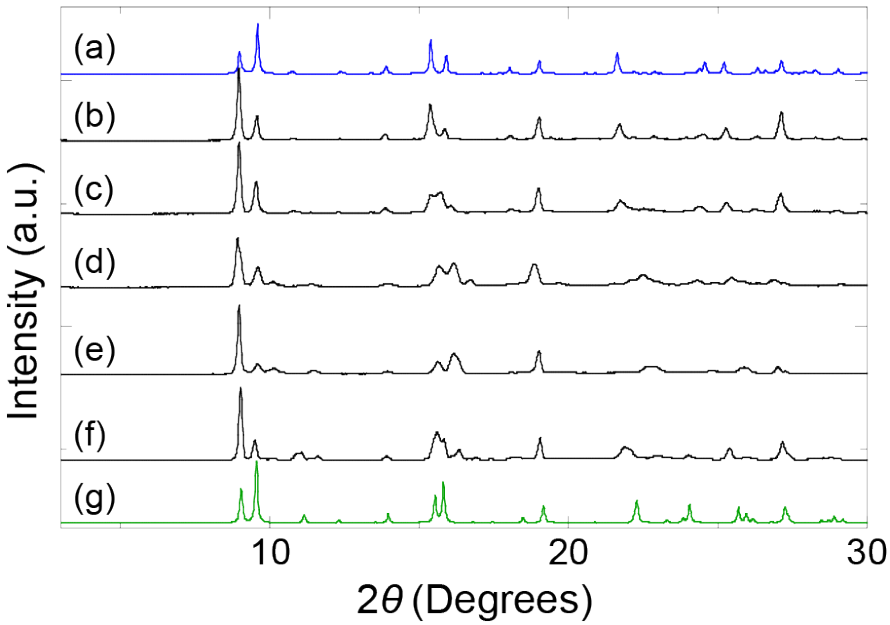

Fig. S18. XRPD patterns of (a) CuCID-1⊃H_2O (simulated†); Zn_xCu_{1-x}CID-1 with (b) x = 0.15, (c) x = 0.33, (d) x = 0.50, (e) x = 0.67, and (f) x = 0.85; and (g) ZnCID-1⊃H_2O (simulated†). (†Note: a and g are simulated profiles from single crystal data).

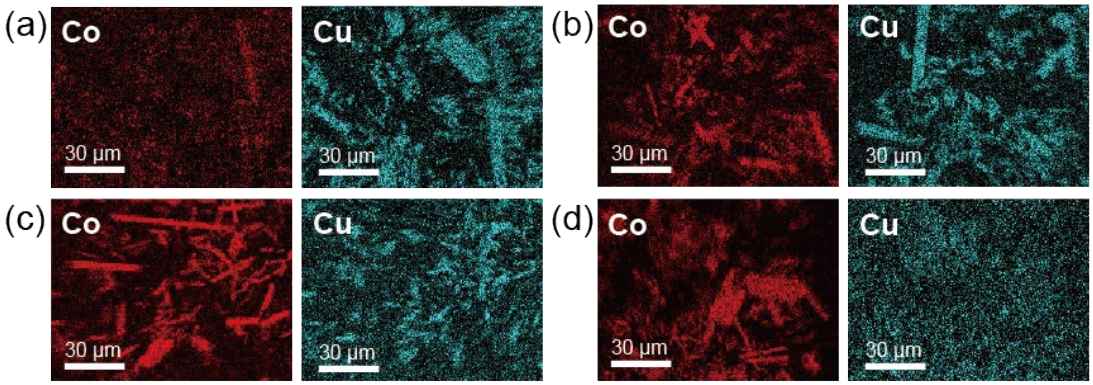

Fig. S19. SEM-EDX images of Co_xCu_{1-x}CID-1 with (a) x = 0.15, (b) x = 0.33, (c) x = 0.67, and (d) x = 0.85.

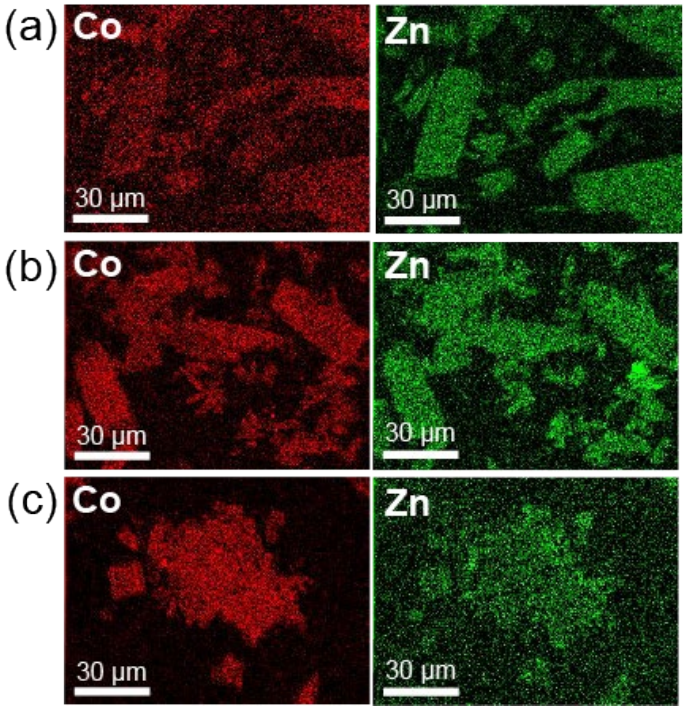

Fig. S20. SEM-EDX images of Zn_xCo_{1-x}CID-1 with (a) x = 0.33, (b) x = 0.67, and (c) x = 0.85.

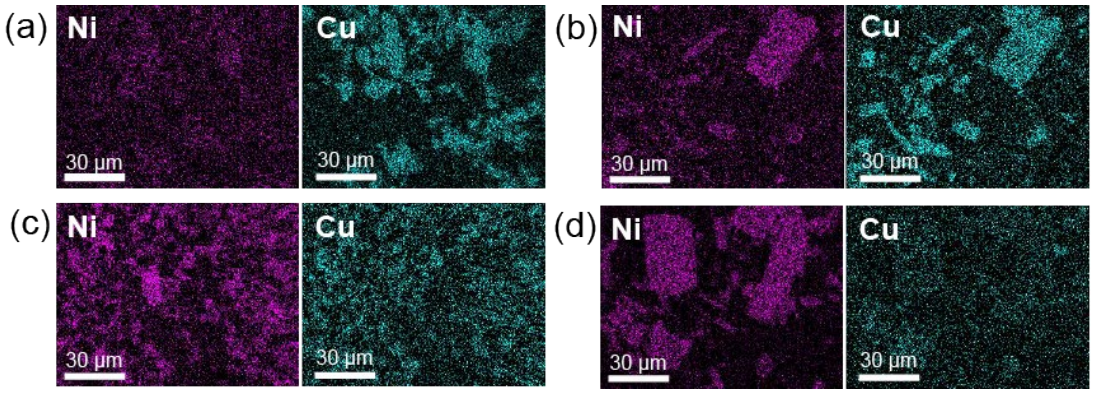

Fig. S21. SEM-EDX images of Cu_xNi_{1-x}CID-1 with (a) x = 0.15, (b) x = 0.33, (c) x = 0.67, and (d) x = 0.85.

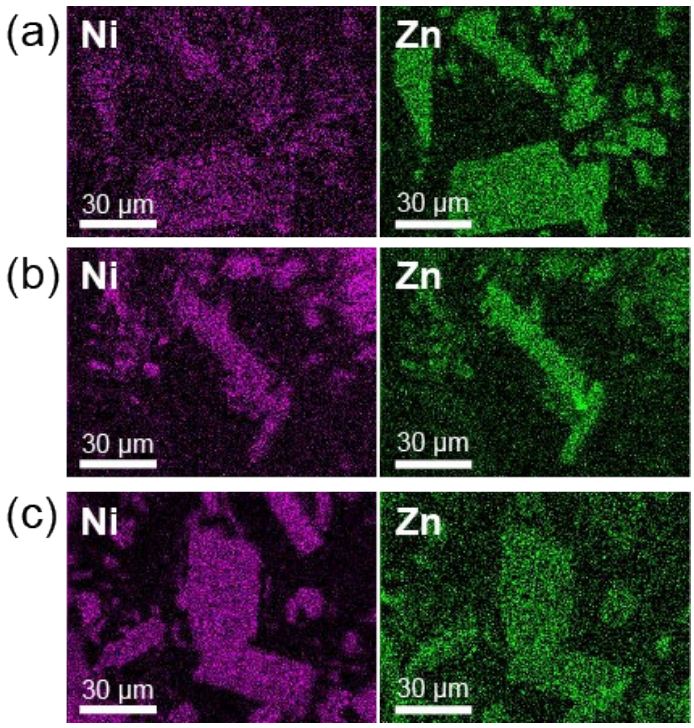

Fig. S22. SEM-EDX images of Zn_xNi_{1-x}CID-1 with (a) x = 0.33, (b) x = 0.67, and (c) x = 0.85.

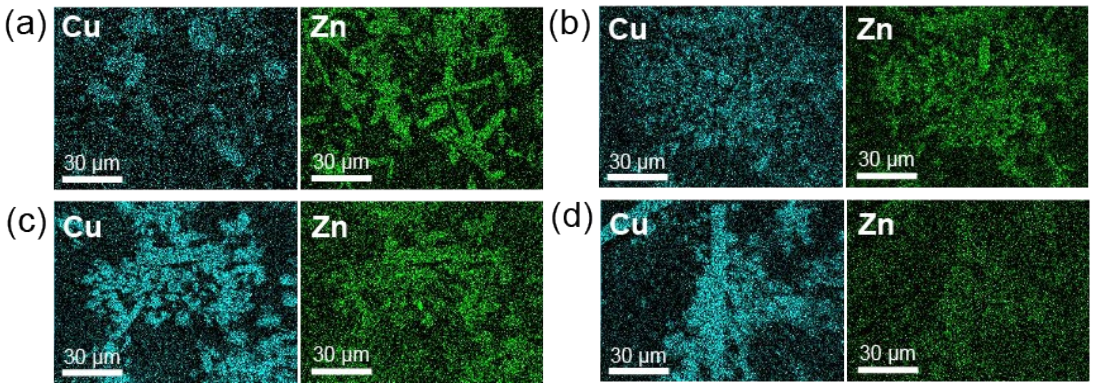

Fig. S23. SEM-EDX images of Zn_xCu_{1-x}CID-1 with (a) x = 0.15, (b) x = 0.33, (c) x = 0.67, and (d) x = 0.85.

S15. Metal content ratio of the $M1_xM2_{1-x}$CID-1 compounds

The metal ratio of as-synthesized $M1_xM2_{1-x}$CID-1 compounds were determined by SEM-EDX.

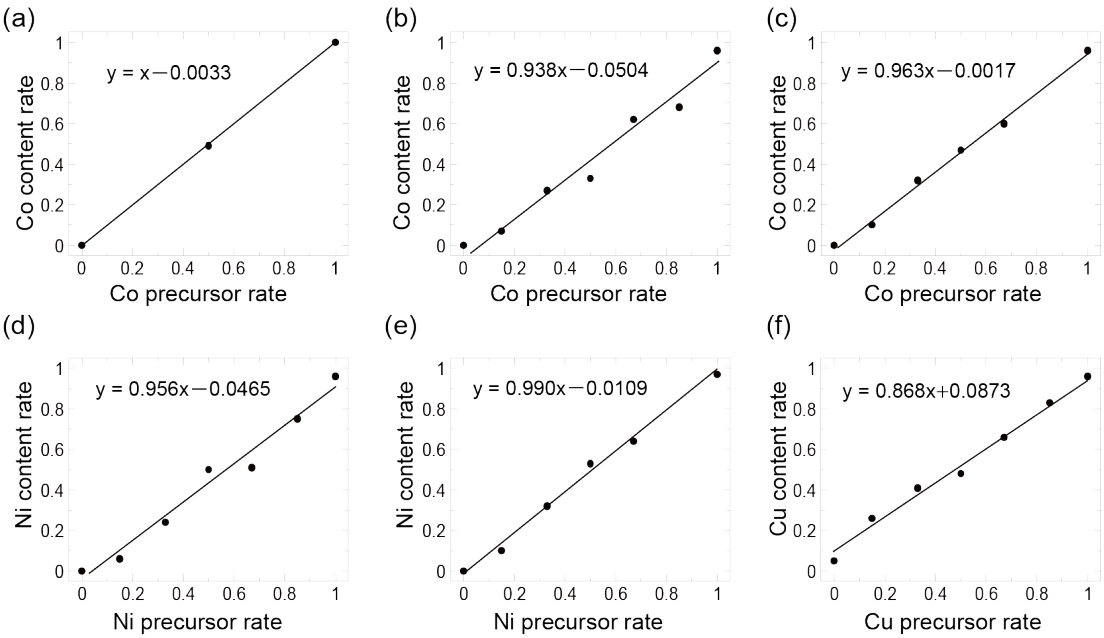

Fig. S24. Metal content ratio of the as-synthesized $M1_xM2_{1-x}$CID-1. (a) Co_xNi_{1-x}CID-1, (b) Co_xCu_{1-x}CID-1, (c) Co_xZn_{1-x}CID-1, (d) Ni_xCu_{1-x}CID-1, (e) Ni_xZn_{1-x}CID-1, and (f) Cu_xZn_{1-x}CID-1.

S16. Possible distribution structures

Solid-solution-type $M1_{0.5}M2_{0.5}$CID-1 with Co, Ni, and Zn ions formed well-mixed solid solutions, as confirmed by their XRPD patterns and SEM-EDX maps. However, their microdistribution structures were not identified. In other words, while the node in CID-1 is a dinuclear complex, the MCID-1 solid-solution exhibits two types of distribution structure: a homo-metal dinuclear structure and one in which both hetero- and homo-metal dinuclear structures are mixed randomly (Figs. S25a and b). We examined the magnetic behaviors of single-metal-ion MCID-1 (M = Co and Ni) and solid-solution-type $M1_{0.5}M2_{0.5}$CID-1 (M = Co, Ni, and Zn) to investigate the structure of the dinuclear part. The results for single-metal-ion MCID-1 (M = Co and Ni) showed that both MCID-1 compounds exhibited paramagnetic behaviors at high temperatures. Furthermore, the value of $\chi_M T$ decreased at low temperatures due to antiferromagnetic Co–Co or Ni–Ni interactions. The behaviors of the solid-solution-type $Co_{0.5}Zn_{0.5}$CID-1 and $Ni_{0.5}Zn_{0.5}$CID-1 are similar to those of CoCID-1 and NiCID-1, respectively (Figs. S25c and d). These results suggest that part of the dinuclear structure is constructed by the same ion species, as shown in Fig. S25a, whereas that of $Co_{0.5}Ni_{0.5}$CID-1 was dramatically different from those of CoCID-1 and NiCID-1 (Fig. S25e). At low temperatures, the $\chi_M T$ value of $Co_{0.5}Ni_{0.5}$CID-1 did not match the average value for CoCID-1 and NiCID-1. This is due to ferromagnetism that is attributable to interactions between Co and Ni. This strongly suggests that heterometal-dinuclear Co–Ni complexes are formed, as shown in Fig. S25b. The differences in the distributions of metal ions in the cluster are explained by the coordination structures of the metal ions in the as-synthesized compounds; as-synthesized ZnCID-1 shows a distorted coordination structure, whereas the coordination structures of the as-synthesized CoCID-1 and NiCID-1 are close to the symmetric octahedral structure. Therefore, $Co_{0.5}Zn_{0.5}$CID-1 and $Ni_{0.5}Zn_{0.5}$CID-1 become segregated to stabilize each coordination structure in the solid-solution.

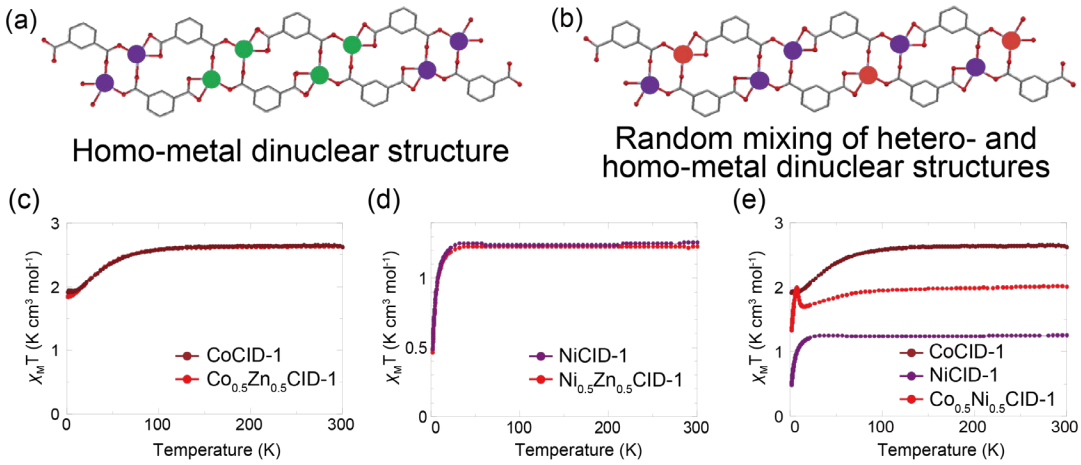

Fig. S25. Possible distribution structures of well-mixed solid-solution CID-1. (a) Homo-metal dinuclear structure and (b) random mixing of hetero- and homo-metal dinuclear structures. Results of magnetic susceptibility experiments: (c) CoCID-1 and $Co_{0.5}Zn_{0.5}$CID-1; (d) NiCID-1 and $Ni_{0.5}Zn_{0.5}$CID-1; and (e) CoCID-1, NiCID-1, and $Co_{0.5}Ni_{0.5}$CID-1.

S17. H_2O-adsorption behavior of $M1_{0.5}M2_{0.5}$CID-1.

We acquired the water-adsorption isotherms for other ratios of $M1_xM2_{1-x}$CID-1 (x = 0.15, 0.33, 0.67, and 0.85) to evaluate the effects of the metal content ratio on the onset pressure and adsorption amount (Fig. S26).

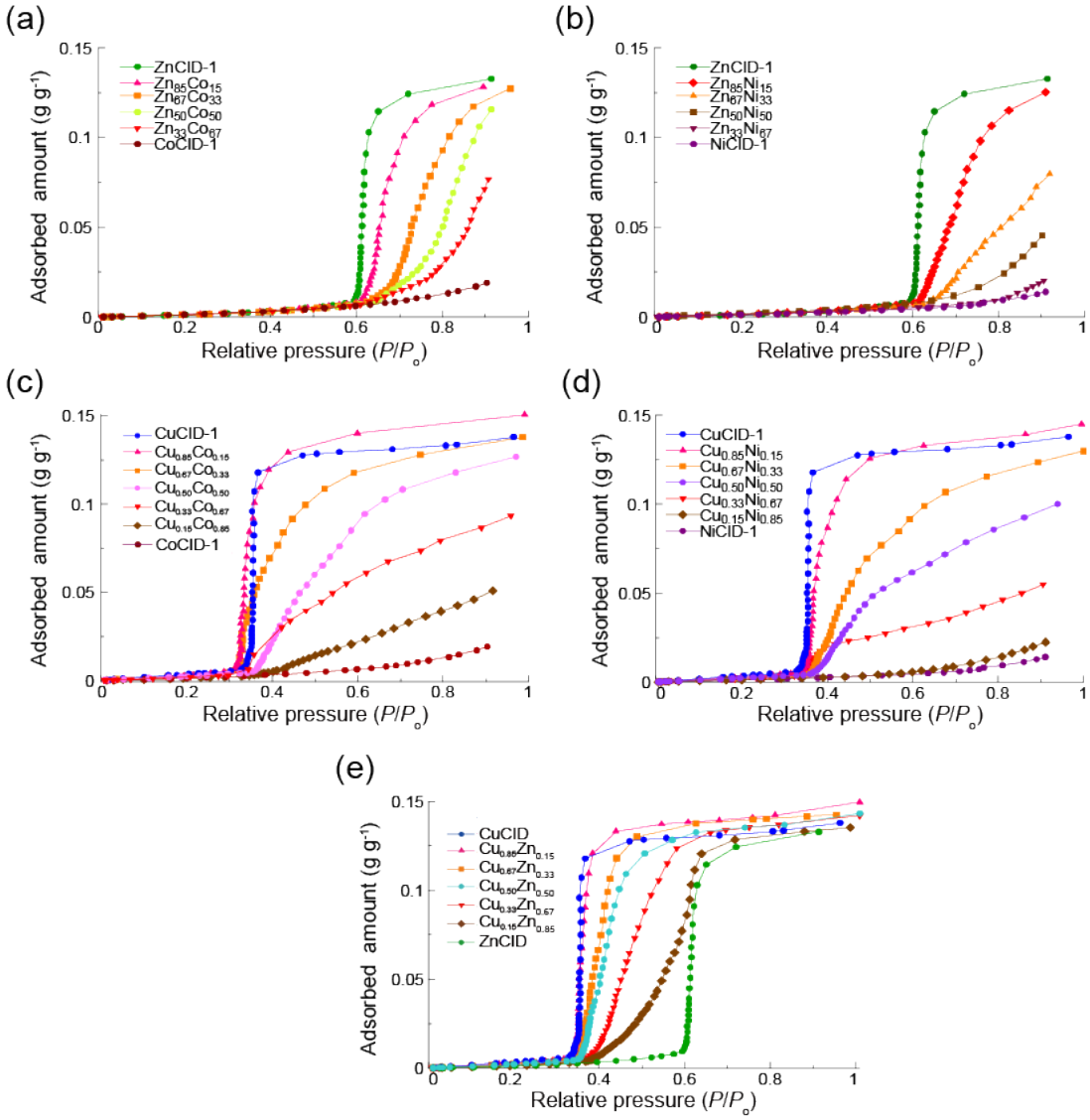

Fig. S26. Water-adsorption isotherms for $M1_xM2_{1-x}$CID-1 at 298 K: (a) Zn_xCo_{1-x}CID-1, (b) Zn_xNi_{1-x}CID-1, (c) Cu_xCo_{1-x}CID-1, (d) Cu_xNi_{1-x}CID-1, and (e) Cu_xZn_{1-x}CID-1.

References

1. L.-F. Song, C.-H. Jiang, C.-L. Jiao, J. Zhang, L.-X. Sun, F. Xu, W.-S. You, Z.-G. Wang and J.-J. Zhao, *Cryst. Growth Des.*, 2010, **10**, 5020.
2. J. Tao, X.-M. Chen, R.-B. Huang and L.-S. Zheng, *J. Solid State Chem.*, 2003, **170**, 130.
3. Y.-H. Wen, J.-K. Cheng, Y.-L. Feng, J. Zhang, Z.-J. Li and Y.-G. Yao, *Inorg. Chim. Acta*, 2005, **358**, 3347.
4. Y. Kamakura, N. Hosono, A. Terashima, S. Kitagawa, H. Yoshikawa and D. Tanaka, *ChemPhysChem*, 2018, **19**, 2134.
5. M. A. Nadeem, M. Bhadbhade, R. Bircher and J. A. Stride, *Cryst. Growth Des.*, 2010, **10**, 4060.